Mon. Not. R. Astron. Soc. **000**, 1–10 (2011) Printed 18 January 2013 (MN LATEX style file v2.2)

Popping star clusters as building blocks of the Milky Way Thick Disc

P. Assmann[1] ⋆, M. Fellhauer[1] †, P. Kroupa[2] ‡, R.C. Brüns[2] §, R. Smith[1] ¶
[1] *Departamento de Astronomía, Universidad de Concepción, Casila 160-C, Concepción, Chile*
[2] *Argelander Institut für Astronomie (AIfA), Auf dem Hügel 71, 53121 Bonn, Germany*

18 January 2013

ABSTRACT
It is widely believed that star clusters form with low star formation efficiencies. With the onset of stellar winds by massive stars or finally when the first super nova blows off, the residual gas is driven out of the embedded star cluster. Due to this fact a large amount, if not all, of the stars become unbound and disperse in the gravitational potential of the galaxy. In this context, Kroupa (2002) suggested a new mechanism for the emergence of thickened Galactic discs. Massive star clusters add kinematically hot components to the galactic field populations, building up in this way, the Galactic thick disc as well. In this work we perform, for the first time, numerical simulations to investigate this scenario for the formation of the galactic discs of the Milky Way. We find that a significant kinematically hot population of stars may be injected into the disk of a galaxy such that a thick disk emerges. For the MW the star clusters that formed the thick disk must have had masses of about $10^6\,M_\odot$.

Key words: Galaxy: disc — Galaxy: formation — Galaxy: kinematics and dynamics — galaxies: star clusters: general — methods: numerical

1 INTRODUCTION

The formation of the Milky Way (MW) galaxy is a mystery unsolved yet. Different models are trying to explain what were the initial conditions that lead to the actual structure of the MW. It is commonly accepted that the structure of the Milky Way, and other comparable disc galaxies, can be divided into three main components, the bulge, the galactic spheroid and the disc. The central bulge has a mass of $\approx 10^{10}$ M$_\odot$ and a characteristic radius of about 1 kpc. The galactic spheroid, which is also called the stellar halo, has a mass of $\approx 3.7 \pm 1.2 \times 10^8$ M$_\odot$ (Bell et al. 2008) and its mass is mostly confined within the the Solar Radius. The stellar halo contains globular clusters, dwarf satellites and their tidal streams, that add up to a mass of about 10^{6-7} M$_\odot$.

For the MW, the disc can be subdivided into at least two parts: the thin disc with a mass of about $M_{\rm disc} = 5 \times 10^{10}$ M$_\odot$, that has exponential radial and vertical scale lengths of approximately $h_{\rm R} = 2.3 \pm 0.6$ kpc (Hammer et al. 2007) and $h_{\rm z} \approx 300$ pc (Juric et al. 2008) respectively. The other part is the thick disk which has scale lengths of $h_{\rm thd,R} = 4.1 \pm 0.4$ kpc and $h_{\rm thd,z} = 0.75 \pm 0.07$ kpc (de Jong et al. 2010). Near the Sun, the thick disc comprises about 6 per cent of the thin disc mass, so that the thick disc mass amounts to $M_{\rm thd} \approx 0.2 - 0.3 \times M_{\rm disc}$. The thick disc is made up mostly of low-metalicity ($[Fe/H] \leqslant -0.4$) stars that have a velocity dispersion perpendicular to the disc plane of $\sigma_{\rm z,obs} \approx 40$ pc Myr^{-1}, compared to the significantly smaller $\sigma_{\rm z}$ of the thin disc, which varies from about $2-5$ pc Myr^{-1} for the young stars (Fuchs et al. 2001). These authors measured the velocity dispersion in the solar neighbourhood as a function of age of the stars. The oldest stars in their sample (CNS4) have about 25 pc Myr^{-1} for 10 Gyr old stars. But then this value might be 'contaminated' by thick disc stars.

Several mechanisms have been proposed to explain the formation of the thick disc in galaxies. One of these mechanisms was proposed by Abadi et al. (2003), who suggest that the formation of the thick disc is the direct accretion of stars from disrupted satellites. The process of accretion occurs approximately at coplanar orbits. Another explanation was suggested by Roŝkar et al. (2008) and Schönrich & Binney (2009), who consider the process of radial migration of the stars. In this mechanism, the stars which end up in the thick disc are trapped onto a resonant co-rotation with spiral arms and may migrate inwards and outwards along the spiral waves. This process conserves angular momentum and does not lead to significant heating of the disc. Another possible scenario is proposed by e.g. Quinn et al. (1993), Kazantzidis et al. (2008) and Villalobos & Helmi (2008) and consists of the thickening of a pre-existing thin disc through minor mergers. The thick disc is formed by the dynamical heating that is induced by satellites merging with a primordial, rotationally supported thin disc. Finally, Brook et al. (2005) and Bornaud et al. (2007) suggest that the formation of the thick disc is triggered in situ. The process of star formation occurs during/after gas rich mergers.

Each model explains different aspects and has its own implications for the disc's kinematical and chemical properties. In the

⋆ E-mail: passmann@astro-udec.cl
† mfellhauer@astro-udec.cl
‡ pavel@astro.uni-bonn.de
§ rcbruens@astro.uni-bonn.de
¶ rsmith@astro-udec.cl

scenario of Abadi et al. (2003), it is possible to distinguish two different dynamics for the orbits of the stars, and they allow one to identify two different components of the disc. The thin disc is a kinematically cold component with stars on circular orbits, and the thick disc is a kinematically hot component with stars with orbital parameters transitional between the thin disc and the spheroid. The nature of the population of stars in the thick disc comes from the tidal debris of satellites, whose orbital plane is roughly coincident with the disc. Their orbits were circularized by dynamical friction prior to their complete disruption.

However, there is evidence for enhanced α-elements abundances in thick-disc stars. This indicates a short star formation time-scale in which enrichment is dominated by Type II supernovae (SNe II) (Alves-Brito et al. 2010; Kobayashi et al. 2011), rather than the slower time-scale expected for dwarf galaxies. In this case, one needs to consider the existence of an active epoch of gas-rich mergers in the past history of galaxy, with the bulk of the thick disc forming in situ (Brook et al. 2005), and strong stellar scattering of clumps formed by gravitational instabilities (Bornaud et al. 2007) (rather than being accreted from satellites) to explain these observations.

During the last years understanding of star formation and star cluster formation has progressed. Now we know that almost all stars form in a clustered mode (e.g. Lada & Lada 2003, and follow-up publications). The star clusters form with low star formation efficiencies and, therefore, they lose a large part of their stars that expand outwards when residual gas is expelled by the action of massive stars. In this context, Kroupa (2002) suggested another mechanism for the formation of the thick disc. Considering the star cluster formation process described above, massive star clusters may add kinematically hot components to galactic field populations, building up, in this way, both galactic discs.

According to the Kroupa (2002) model, the velocity dispersion of the stars in expansion (the new field population) is related with the mass of the initial star cluster, with its radius and also with the efficiency of star formation (Eq. 1 in Kroupa 2002). It is proportional to the square root of the mass of the star cluster, such that heavier star clusters will generate a field population that presents higher dispersion velocities. Thus, a simple estimate suggests that clusters of mass near $10^{5.5}$ $\mathrm{M}_\odot$ may contribute new field populations that have a velocity dispersion of about 40 pc Myr^{-1} which is similar to the velocity dispersion of the thick disk.

In this work we perform numerical simulations to investigate this scenario for the formation of both galactic discs of the Milky Way. To accomplish this investigation we use star clusters of different masses and we consider their disruption under distinct low star formation efficiencies (we refer to such clusters as popping star clusters). We place the star cluster on an orbit around the Galactic Centre at the Solar Radius of 8.5 kpc and observe how the stars of these star clusters distribute themselves in the potential of the MW.

In the next Section we describe the detailed setup of our investigation and describe our results in Section 3. We discuss our findings in the last Section (4).

2 SIMULATIONS

2.1 Code Description

We simulate the popping star cluster using the particle mesh code SUPERBOX (Fellhauer et al. 2000), which has moving high-resolution sub-grids, which stay focused on the star cluster. These sub-grids provide high spatial resolution at the place of interest. A particle-mesh code neglects by default close encounters between the particles (which are rather representations of the phase-space than actual single stars) and is therefore called collision-less. With a collision-less code it is possible to simulate galaxies without having to use the actual number of stars (10^{10}). A code as SUPERBOX is in principle unsuitable to simulate star clusters, as with them two-body relaxation effects are important and govern their evolution. In our study we dissolve the star clusters immediately, dispersing their stars within a short time (a few crossing times) into the overall potential of the MW, therewith being in a regime where near encounters between stars do not play any rôle. Now the ability of SUPERBOX to model particles with arbitrary masses gives us the possibility to sample the phase space (e.g. by using more particles than actual stars in the star cluster) more precisely.

The code is fast and resource-efficient, i.e. it requires a small amount of computer memory. Therefore, this code enables its user to simulate objects with millions of particles, with high resolution, and it can run on normal desktop computers.

SUPERBOX has two levels of high resolution sub-grids. The highest resolution grid has a resolution (i.e. cell-length) of 0.2 pc and covers the initially dense SC completely. The medium resolution grid has a cell-length of 40 pc and covers the complete z-height of interest. Finally the outermost grid covers the complete orbit of the SCs around the centre of the MW with a resolution of 0.4 kpc.

Regarding the fixed time-step of SUPERBOX we choose initially a value to ensure that the SCs are kept stable without further influence. Therefore the time-steps were different for the different masses ranging from 0.03 Myr for the 10^4 $\mathrm{M}_\odot$-clusters, via 0.01 and 0.006 Myr to 100 yr (0.0001 Myr) for the most massive clusters (10^7 $\mathrm{M}_\odot$). As these tiny time-steps require very long simulation times until we finally would reach 10 Gyr, we check the simulations and stop them as soon as the SCs are completely dissolved. When all stars are unbound and just traveling under the influence of the global potential, we restart the simulations with a larger time-step of 0.5 Myr.

2.2 Set-up

We consider the following set-up for our simulation. The potential of the MW is modeled as an analytical background potential consisting of a Hernquist sphere to generate the bulge,

$$\Phi_{\mathrm{bulge}}(r) = -\frac{GM_{\mathrm{b}}}{r+a}, \tag{1}$$

using $M_{\mathrm{b}} = 3.4 \times 10^{10}$ $\mathrm{M}_\odot$ and $a = 0.7$ kpc, the Miamoto-Nagai model to mimic the disc,

$$\Phi_{\mathrm{disc}}(r) = -\frac{GM_{\mathrm{d}}}{\sqrt{R^2 + (b + \sqrt{z^2 + c^2})^2}}, \tag{2}$$

with $M_{\mathrm{d}} = 10^{11} M_\odot$, $b = 6.5$ kpc and $c = 0.26$ kpc. Finally, we use a logarithmic potential to account for the rotation curve of the MW disk,

$$\Phi_{\mathrm{halo}}(r) = \frac{v_0^2}{2} \ln(r^2 + d^2) \tag{3}$$

with $v_0 = 186$ km s^{-1} and $d = 12$ kpc. The superposition of these components gives a good analytical representation of the Milky Way potential today. The potential of the MW is kept constant throughout the simulation. This is highly idealised as we expect the Galaxy to grow and evolve over this period of time. We discuss this issue further in Sect. 4.

Table 1. Initial conditions of the Plummer spheres which represent the star clusters for each simulations. The first column shows the initial Plummer radius of the star clusters, the second the initial mass of the sphere and the third the initial characteristic velocity dispersion. Finally the fourth and fifth columns represent the SFE and the final mass after gas expulsion.

$R_{\rm pl}$ [pc]	$M_{\rm ecl}$ [$M_\odot$]	$\sigma_{\rm ecl}$ [kms^{-1}]	SFE [%]	$M_{\rm f}$ [$M_\odot$]
1	2.2×10^4	5.28	40	8.80×10^3
1	2.2×10^4	5.28	20	4.40×10^3
1	2.2×10^4	5.28	1	0.22×10^3
1	2.2×10^5	16.7	40	8.80×10^4
1	2.2×10^5	16.7	20	4.40×10^4
1	2.2×10^5	16.7	1	0.22×10^4
1	2.2×10^6	52.8	40	8.80×10^5
1	2.2×10^6	52.8	20	4.40×10^5
1	2.2×10^6	52.8	1	0.22×10^5
1	2.2×10^7	166.8	40	8.80×10^6
1	2.2×10^7	166.8	20	4.40×10^6
1	2.2×10^7	166.8	1	0.22×10^6

The single cluster is represented by a Plummer (1911) sphere. Even though, this might not be the most ideal representation of a young embedded star cluster, the Plummer distribution has the advantage that all quantities are easily accessible with analytical formulas. And it is in fact a better representation of a young, newly formed star cluster (Kroupa 2008), which has not yet been tidally truncated, than e.g. a King profile. The Plummer profile has two free parameters to choose, namely the Plummer radius, which we keep fixed at $R_{\rm pl}=1$ pc, and the total mass of the Plummer sphere – a parameter which is varied in this study. All other quantities (e.g. crossing-time, velocity dispersions, distribution of velocities) are then simple functions of the two input parameters. The choice of the small Plummer radius is based on observations of embedded star forming regions (Kroupa 2008). Furthermore we choose a cutoff radius of 5 pc. The choice of the cut-off radius is justified by the fact that beyond $5R_{\rm pl}$ there is only less than 2 per cent of the total mass of the Plummer model missing. Each cluster has an initial mass of $M_{\rm ecl}=2.2\cdot10^4$, $2.2\cdot10^5$, $2.2\cdot10^6$ and $2.2\cdot10^7$ $M_\odot$ respectively leading to an initial crossing time of 0.6 Myr, 0.2 Myr, 0.06 Myr and 0.001 Myr and is represented with $2,500,000$ particles.

This configuration, placed on a circular orbit at the Solar Radius of 8 kpc, suffers from the process of gas expulsion. This process is mimicked by artificially reducing the mass of each particle according to the SFE used. We investigate a range of possible SFEs namely 0.4, 0.2 and 0.01.

Finally, we also use two distinct ways, how this mass-loss progresses. We perform simulations with an instant mass-loss and simulations where the mass in gas is lost during the time-interval of one crossing time of the star cluster.

As the simulation time we choose a time-span of 10 Gyr to ensure that the particles have enough time to disperse into a stable configuration in the Galactic potential.

3 RESULTS

3.1 z-distribution of the stars

In Fig. 1, we show the number of stars with respect to their z-height after 10 Gyr of simulation time. Therefore, we count all stars in a vertical cylinder of 40 pc radius around the Sun. To increase the statistical significance and also because we do not know the actual position of the star cluster with respect to the Sun (except that they have by design the same Galacto-centric distance), we actually count the stars in an 80 pc wide ($7.96\leqslant R=\sqrt{x^2+y^2}\leqslant 8.04$ kpc) ring around the galaxy and plot the z-height of the stars in Fig. 1. We choose to simulate until 10 Gyr to ensure that the objects had enough time to evolve slowly into an equilibrium. The SCs at this stage are completely dissolved in almost all of the cases.

Table 2. Results of the simulations. The first three columns represent the initial mass of the star clusters, the SFE used and finally if the gas was expelled instantaneously 0 or over a crossing-time 1 (GET = gas expulsion time). The fourth and fifth column represent the scale height of the thin and thick disc, respectively, after 10 Gyr of simulation. The last line represents our combined model (see main text).

$M_{\rm ecl}$ [$M_\odot$]	SFE [%]	GET [$t_{\rm cr}$]	$h_{\rm z,thin}$ [pc]	$h_{\rm z,thick}$ [pc]
2.2×10^4	40	0	9.0	—
2.2×10^4	40	1	10.1	—
2.2×10^4	20	0	13.0	—
2.2×10^4	20	1	10.0	—
2.2×10^4	1	0	16.4	—
2.2×10^4	1	1	16.0	—
2.2×10^5	40	0	25.0	—
2.2×10^5	40	1	31	—
2.2×10^5	20	0	42.4	—
2.2×10^5	20	1	35.6	—
2.2×10^5	1	0	56.0	—
2.2×10^5	1	1	47.0	—
2.2×10^6	40	0	27.0	130
2.2×10^6	40	1	14.2	110
2.2×10^6	20	0	35.2	170
2.2×10^6	20	1	33.3	149
2.2×10^6	1	0	39.0	215
2.2×10^6	1	1	31.3	183
2.2×10^7	40	0	31.3	500
2.2×10^7	40	1	51.3	500
2.2×10^7	20	0	71.3	568
2.2×10^7	20	1	70.0	529
2.2×10^7	1	0	67.0	676
2.2×10^7	1	1	76.0	704
8.8×10^7	20	1	17	540

The different rows of Fig. 1 correspond to the three different SFEs we adopt. The top row shows the results of our SCs having 40 per cent of SFE, the middle row the results of the 20 per cent simulations and finally the bottom row the results obtained with the extremely low efficiency of only 1 per cent. The left column shows simulations where the gas-removal time was one crossing-time of the star cluster, while the right column represents the final distribution of stars when the gas was removed instantaneously. The curves, in each panel, from left to right correspond to the star distributions of star clusters which had an initial mass of $M_{\rm ecl}=2.2\times10^4$ $M_\odot$ (black on-line), 2.2×10^5 $M_\odot$ (red on-line), 2.2×10^6 $M_\odot$ (green on-line) and finally 2.2×10^7 $M_\odot$ (blue on-line).

First we check our results for a dependency on the under-lying analytic disc potential (Miamoto-Nagai model). For this reason we compare different fitting functions to our distributions. One would expect that if the under-lying potential had any influence it would

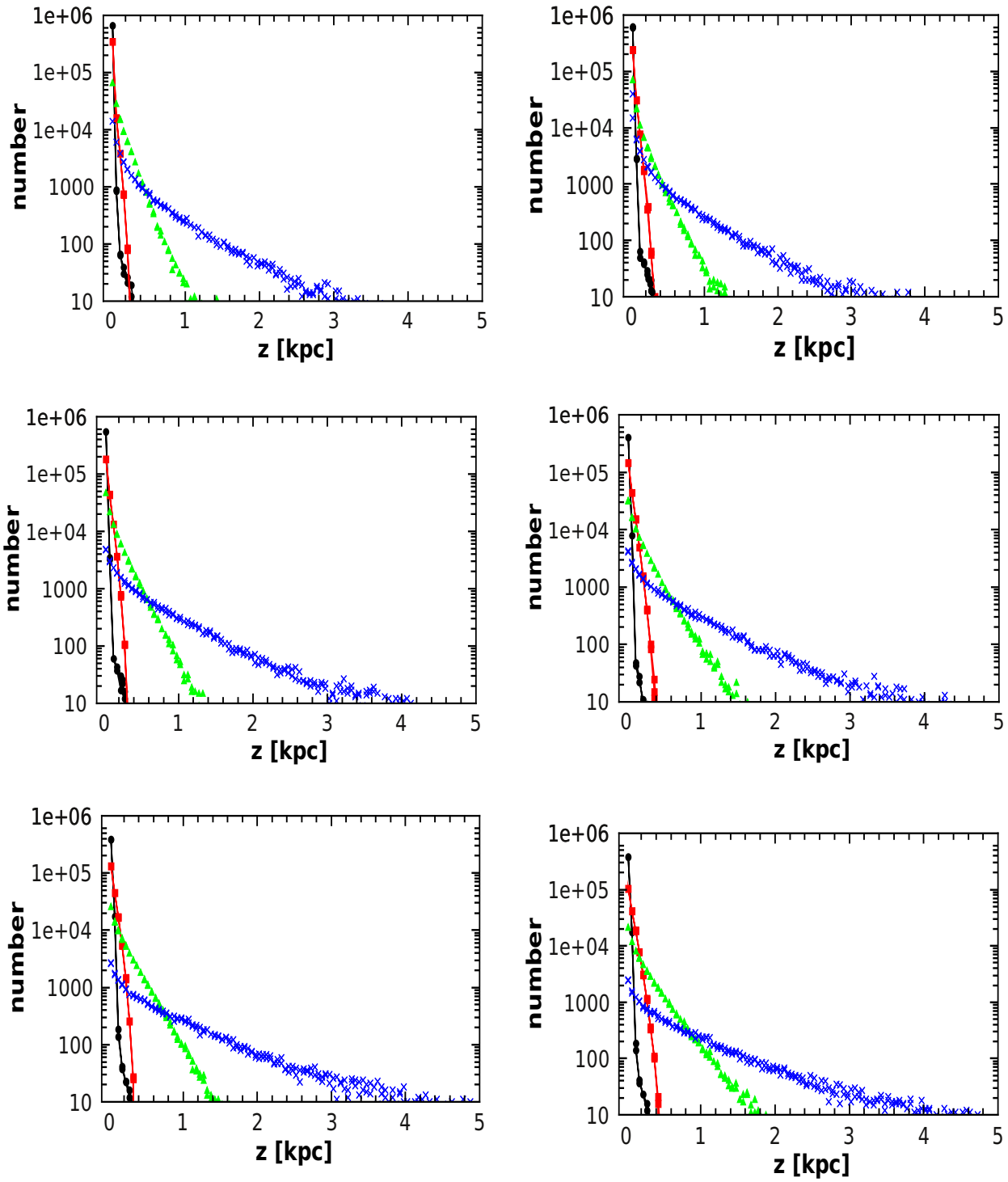

Figure 1. The z-distribution of particles of the dissolved star clusters after 10 Gyr of simulation time. From top to bottom we show the results of the different SFEs (0.4, 0.2 and 0.01). Left panels are for the gas-expulsion during a crossing-time and right panels show the results for instantaneous gas-expulsion. Inside each panel the curves from left to right represent the results of the different initial masses of the star clusters namely $M_{\rm ecl} = 2.2 \times 10^4$ M$_\odot$ (circles black on-line), 2.2×10^5 M$_\odot$ (squares red on-line), 2.2×10^6 M$_\odot$ (triangles green) and finally 2.2×10^7 $M_\odot$ (crosses blue).

be visible in form of a similar distribution of the dispersed stars, i.e. in our case a Plummer like distribution, as the Miamoto-Nagai potential is a flattened version of the Plummer potential. But our results showed that the best fitting functions were either a single or a double exponential. Therefore we are quite confident, that our results are not influenced by the particular choice of the analytical potential.

The results show no difference with respect to the method of gas- (mass-)loss we applied. The final configurations are similar

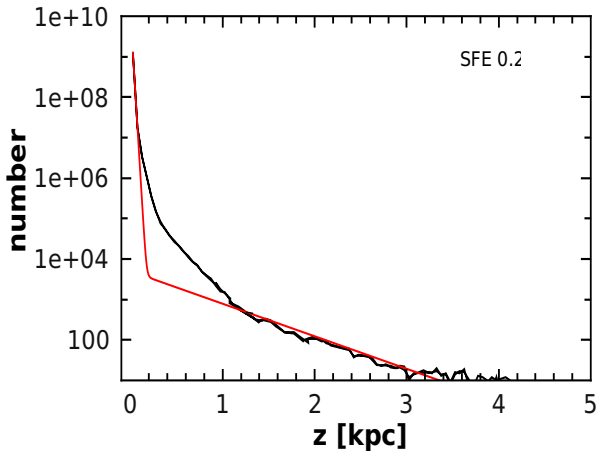

Figure 2. Distribution of stars in the z-direction if we add our different mass clusters according to a standard ICMF. Fitting line is a double exponential.

irrespective if we remove the gas instantaneously or more smoothly during a crossing-time of the star cluster.

But we see immediately a strong dependency on the initial mass of the star cluster. Low mass clusters (2.2×10^4 M$_\odot$ and 2.2×10^5 M$_\odot$) disperse their stars only close to the Galactic plane and therefore can only contribute to the build-up of the thin disc. This changes as soon as we look at the high mass clusters (2.2×10^6 M$_\odot$ and 2.2×10^7 $M_\odot$). These clusters are able to distribute their stars out to 1–4 kpc in z-height and therefore could be the building blocks of the thick disc.

Finally the SFE has only a second order effect on the final distribution. The lower the SFE the wider is the spread of the final particle distribution. The reason is quite simple as a lower SFE means that the initially binding potential of the embedded cluster is deeper such that the stars, which amount to a mass M say, move more rapidly within it. The same stellar mass, M, but confined by a less-massive gas potential (being equivalent to a higher star-formation efficiency), has a smaller velocity dispersion before the gas is removed. One also has to note that even though a SFE of 0.4 should in principal lead to a surviving remnant star cluster, for all masses except our highest mass models, these remnants were not massive enough to survive the whole 10 Gyr of simulation time. With a SFE of 0.4 the cluster still 'pops' but instead of dissolving completely a small fraction of stars re-virialises into a bound star cluster. Kroupa et al. (2001) performed high-precision Nbody modelling of this process explaining that a pre-Orion Nebula Cluster evolves into a Pleiades type cluster whereby $2/3$rds of the population "pop away". The majority of stars thus gets distributed as unbound stars inside the MW potential. The fraction of stars which remains bound is a function of the SFE. For the low-mass cases this bound remnant does not survive the tidal forces of the MW for very long. Only the more massive remnants stemming from massive initial clusters are able to survive the full 10 Gyr. The future fate of these remnants is of no concerns in our study, as our code is not able to describe the internal dynamics of star clusters over long time intervals correctly.

As stated above we then fitted exponential functions to the obtained star distributions in z-direction. For all models we tried to fit a single exponential of the form:

Table 3. W-velocity dispersions of our dissolving star clusters. The first three columns are the same as in Tab. 2. We then give the fitted values for the dispersion using the method described in the main text for the thin and thick disc component. The last column is the FWHM of the whole distribution. Low mass star clusters, which only contribute to the thin disc have only one value fitted. Last line is the result of our combined model using an ICMF.

$M_{\rm ecl}$ [M$_\odot$]	SFE [%]	GET [$t_{\rm cr}$]	$\sigma_{\rm z,thin}$ [km s^{-1}]	$\sigma_{\rm z,thick}$ [km s^{-1}]	FWHM [km s^{-1}]
2.2×10^4	40	0	1.04	—	1.0
2.2×10^4	40	1	0.78	—	1.0
2.2×10^4	20	0	1.59	—	1.2
2.2×10^4	20	1	1.24	—	1.0
2.2×10^4	1	0	1.98	—	1.1
2.2×10^4	1	1	1.98	—	1.1
2.2×10^5	40	0	1.27	—	1.0
2.2×10^5	40	1	1.26	—	1.4
2.2×10^5	20	0	2.36	—	1.3
2.2×10^5	20	1	2.03	—	1.3
2.2×10^5	1	0	2.80	—	1.3
2.2×10^5	1	1	2.61	—	1.3
2.2×10^6	40	0	3.28	20.0	5.9
2.2×10^6	40	1	4.10	17.5	2.3
2.2×10^6	20	0	4.50	24.2	1.5
2.2×10^6	20	1	4.01	20.5	1.5
2.2×10^6	1	0	4.30	27.3	2.1
2.2×10^6	1	1	4.55	23.6	1.7
2.2×10^7	40	0	6.28	58.8	6.0
2.2×10^7	40	1	5.42	59.2	5.0
2.2×10^7	20	0	7.36	58.3	7.0
2.2×10^7	20	1	6.10	50.2	6.0
2.2×10^7	1	0	12.9	69.8	12.0
2.2×10^7	1	1	8.71	69.3	8.0
8.8×10^7	20	1	1.26	79.8	1.26

$$\rho(z) = \rho_{0,\rm thin} \cdot \exp\left(\frac{z}{h_{\rm z,thin}}\right), \quad (4)$$

where $h_{\rm z,thin}$ represents the z-scale height of the thin disc and compared the results with the ones obtained if we used a double exponential function of the form:

$$\rho(z) = \rho_{0,\rm thin} \cdot \exp\left(\frac{z}{h_{\rm z,thin}}\right) + \rho_{0,\rm thick} \cdot \exp\left(\frac{z}{h_{\rm z,thick}}\right), \quad (5)$$

where $h_{\rm z,thick}$ is the z-scale height of the thick disc. The fitted values of $h_{\rm z,thin}$ and $h_{\rm z,thick}$ are shown in Tab. 2. For the low mass clusters the best fit was always the single exponential fit, while for the high mass clusters the distribution was better fitted with a double exponential. In the table we only give the values for the best fit of the two fitting functions adopted. Again it is clear that the method of removing the gas has no influence on the final distribution. But we see a clear trend towards larger scale-lengths by increasing the cluster mass and by lowering the SFE. For an example, in the case $M_{\rm ecl} = 2.2 \times 10^6$ M$_\odot$ and a SFEs of 40% or 20%, the z scale-height of the thin disc is about 14 pc. Using a SFE of only 1 per cent gives a z-scale height of 16–18.2 pc. The same type of behavior can be observed for the thick discs.

We should make clear that the actual distribution of stars is neither a perfect single nor a perfect double exponential distribution. With the low-mass clusters we only see a thin distribution like a 'peak' and only few stars in a sort of 'envelope' but with

low z-heights. Therefore a single exponential fits the data well. For high-mass clusters we see this 'peak' as well together with a very extended structure (the 'envelope') reaching out to large z-heights. These clusters are able to spread out their stars to large radii. For those distributions a double exponential fits the data better.

Even though none of the values from Tab. 2 come anywhere close to the values of the thin and thick disc of the MW, it is astonishing that our high-mass clusters distribute their particles automatically into a distribution which is best fitted by a double exponential, i.e. show the same shape as the actual distribution of MW stars. The low numbers can easily be understood by the fact that the MW is not made out of one single dispersed star cluster at one certain time and on one certain orbit. We rather have an overlay of star clusters forming with different masses at different times and on all radial distances. Furthermore, we do not take any further effect into account which could enhance the vertical spread of the star particles, e.g. scattering with giant molecular clouds or spiral arms, adiabatic heating due to the growth in mass of the MW disk.

3.1.1 Combined model

To at least asses the influence a generation of star clusters would have onto the results we build our combined model by assuming an initial cluster mass function (ICMF). The ICMF is a fundamental property of the process of star formation in galaxies (Kroupa & Boily 2002). It gives the number of star clusters in a certain mass interval $dM_{\rm ecl}$ which form during one event of star formation,

$$N(M_{\rm ecl}) \propto M_{\rm ecl}^{-\beta} dM_{\rm ecl}, \quad (6)$$

where β is the spectral index of cloud mass spectrum. In this work we use $\beta = 2$, because this value was measured for young star clusters in the Antennae (Whitmore et al. 1999) and generally by Weidner & Kroupa (2004). Because we use a particle-mesh code, where particles represent phase-space elements and not single stars, all of our model clusters have the same number of particles, irrespective of their mass. We therefore are able mimic an ICMF with a power law index of $\beta = 2$ by co-adding our results using a power of $\beta - 1 = 1$ only, to ensure that every particle has the correct weight in the combined model.

The density distribution of the disrupted star clusters at $10\ Gyr$ using the ICMF is shown in Fig 2. In this figure we consider star clusters with a SFE of 20% and where the gas expulsion happens during a crossing time. One clearly sees that the shape of the density distribution has a similar resemblance as the thin and thick disc of the MW. We fit a double exponential function given by Eq. 5 and obtain values for the z scale-heights of $h_{\rm z,thin} = 50$ pc for the thin disc and $h_{\rm z,thick} = 500$ for the thick disc (see also last line of Tab. 2). These values are now much closer to the real values of the MW and therefore we believe that by adding also additional scattering and multiple star formation events, we may be able to account for the real discs of the MW.

3.2 W-velocity distributions

In addition to studying the shape of the z-distribution of the stars, we can also use our simulations to look at the velocity space. Table 3 shows the velocity dispersion obtained for all our simulations by fitting straight lines to the probability plot of W-velocities (velocity in z-direction), as described in Bochanski et al. (2007). The probability plot is a graphical technique where we plot the cumulative probability distribution in units of the standard deviation of the distribution. When the distribution is a Gaussian, it shows as a straight line in the probability plot with a slope corresponding to the standard deviation. The y-axis-intercept is equal to the median of the distribution. When the distribution is non-Gaussian, the plotting line deviates from a straight line. We are therefore able to fit two separate lines to the inner and outer parts of the distribution, resembling the velocity dispersion for the thin and thick disc component of our models. Again, we note that our low-mass models only contribute to the thin disc component.

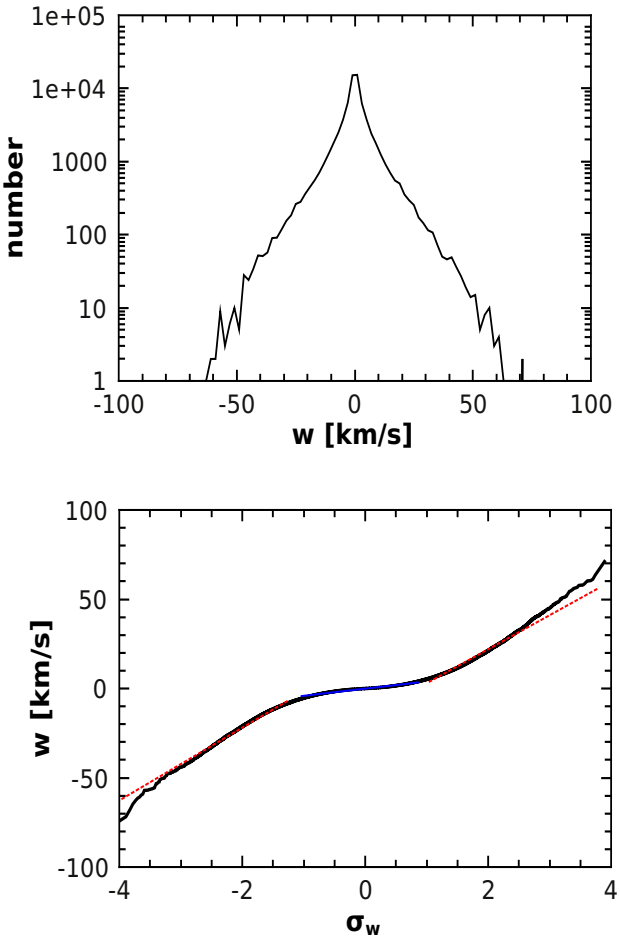

Figure 3. In the top panel we show the W-velocity distribution of one of our high mass models (see main text). One clearly sees the non-Gaussianity of the distribution. The lower panel shows the probability plot for this distribution with two straight lines fitted to the inner and outer parts respectively, giving the velocity dispersion for the two parts.

As example we show the velocity distribution and its probability plot for a high mass model in Fig. 3. It shows a star cluster with a SFE of 20 % and a mass of 2.2×10^6 $M_\odot$. Clearly, the velocity distribution of the stars is not a Gaussian at all. Also two Gaussians will not represent this kind of distribution fully. But it shows clear similarities with the velocity distribution of stars found in the MW (Bochanski et al. 2007). So even though we have an overlay of an undefined number of Gaussians we perform the same analysis as observers and fit straight lines to the inner and outer parts of the probability plot. The probability plot is well fitted with two lines: low dispersion velocities ($<|\ 1\sigma\ |$), from the population of stars confined to the thin disc, and high dispersion velocities ($>|\ 1\sigma\ |$),

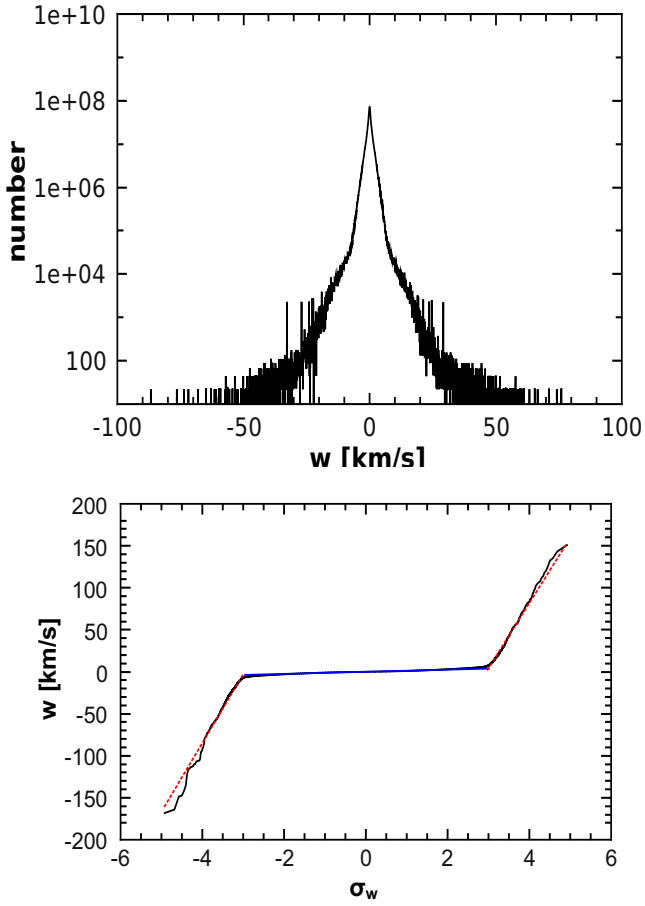

Figure 4. Same as Fig. 3 but now for our combined model using an ICMF as described in the main text.

where the population of the stars corresponds to the thick disc. In our example, the slope for the velocity dispersion for the stars of the thin disc is 4.01 km s^{-1} and for the thick disc stars 20.5 km s^{-1}.

Additionally we measure the full width half maximum of the velocity distribution and give these values as the last entry in Tab. 3.

If we compare the velocity dispersions of the initial star clusters with the dispersions we measure of the dispersed stars we see the following effects:

- The dispersion of the dispersed stars is always significantly lower than the initial dispersion inside the star cluster.
- The ratio of final to initial velocity dispersion decreases with increasing mass (i.e. initial dispersion) of the star cluster.
- This fraction is higher for the stars in the thick disc component.
- We get higher dispersions for a given initial cluster mass, if the SFE is lower. The reason is that the stars at lower SFEs have a smaller potential barrier to cross.
- If the initial mass of the star cluster is about 10^6 M$_\odot$ the velocity distributions are better fitted by two Gaussians than just one; similar to the z-distributions.

Table 4. Ratio between initial velocity dispersion of the star clusters and the final velocity disspersion of the dispersed stars. Shown are the models with a SFE of 0.01 and instanteneous gas-expulsion only.

initial mass [M$_\odot$]	final σ [km s^{-1}]	initial σ [km s^{-1}]	ratio
2.2×10^4	2.0	5.3	0.38
2.2×10^5	2.8	16.7	0.17
2.2×10^6	27.3	52.8	0.52
2.2×10^7	69.8	166.8	0.42

3.2.1 Combined model

As with the $z-$distribution we now investigate how our results change if we adopt an ICMF. We combine our models the same way as done for the z-distribution and show the combined velocity distribution in the top panel of Fig. 4 (and also in the last line of Tab. 3). The derived probability plot to this distribution is shown in the lower panel of Fig. 4. Fitting straight lines to the inner and outer parts give velocity dispersions of 1.3 and 80 km s^{-1} for the thin and thick disc component respectively.

As we can see, the velocity dispersion is much larger in the thick disc than in the thin disc. Comparing our values of the solar neighborhood with published observations (Bensby et al. 2003; Vallenari et al. 2006; Veltz et al. 2008), which report $\sigma_{\rm w,thick} = 38$ km s^{-1} and $\sigma_{\rm w,thin} = 16$ km s^{-1} for the thick disc and thin disc respectively, shows that we underestimate the thin disc values quite substantially and overestimate the value for the thick disc. An explanation could be that we do not take any other scattering mechanisms into account, which would elevate our thin disc dispersion. For the thick disc it could probably be, that there never were any SCs with 10^7 M$_\odot$ formed in the history of the MW. These high-mass clusters are mainly responsible for the elevated velocity dispersion in the thick disc component of our models.

3.3 Of Christmas trees and azimuthal fish

One interesting result can be observed in our simulation when we focus on the z-distribution of the stars at early stages (< 1 Gyr) of the SC evolution. For an example, in Fig 5 we show the z-distribution of the stars, after 270 Myr, for the simulation with an initial mass of 2.2×10^7 M$_\odot$ and a SFE of 0.2.

The shape of the z-distribution looks like a Christmas tree (this effect was seen in our simulations shortly before Christmas 2009). The origin of this shape can be explained by considering the dynamical processes during the SC evolution. The star cluster is orbiting on a circular orbit around the Galactic Centre. After gas expulsion, some of the stars acquire higher expanding velocities and form the thick disc. We show in Fig 6 in the top left panel the W-velocity distribution as a function of the distance between 8 and 9 kpc from the Galactic Centre after 270 Myr (i.e. about one orbital period). The velocities show discrete layers. A similar behaviour is also described in Küpper et al. (2010) where the tidal tails of SCs show density enhancements with regular spacings stemming from the turn-around points of the escaped stars on epicycles. We suspect that our Christmas tree has a similar explanation and is due to the turn-around points of stars on their z-oscillations (z-epicycle). Küpper et al. (2010) report that their star clusters have to be sufficiently long lived to show this behaviour in their tidal tails, while we see this effect very early in the evolution of our models. The reason for this difference is quite simple. In the simulations of Küpper et al. (2010) the star clusters are in virial equilibrium and

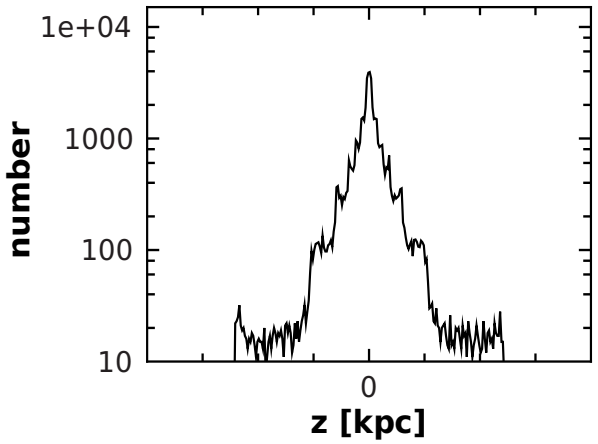

Figure 5. Example for a Christmas tree as found in all of our simulations. It is a peculiar transient feature seen only after one revolution around the galaxy ≈ 270 Myr (also the simulation time shown in the figure). It disappears after a few revolutions more.

loose stars through tidal and two-body effects quite slowly. Therefore it needs a long time for the tidal tails to form and evolve. Thus, in the Küpper et al. (2010) case the epicyclic motions of stars evaporating from star clusters are nearly coherent or in-phase since the stars leave the cluster with very similar and small velocities. The popping clusters, on the other hand, expel stars with a larger range of velocities within a short time-span.

The middle and lower left panel of Fig. 6 show that we only see this phenomenon in the W-velocities, while U (radial velocity) and V (azimuthal velocity) show a simple bulk motion (except for a few stars which lag behind). This special appearance of the Christmas tree gets later erased and transformed into a smooth distribution as described in Sect. 3.1. Also the velocities in W do not show the quantized behaviour any longer as we can see in the top right panel of Fig. 6. The transient tree feature more or less disappears when the stars which form the leading arm of the tidal tails wrap all around the whole orbit and start to overlap with the trailing stars filling the gaps in velocity space. A deeper theoretical explanation for this astonishing feature is not part of this paper and will be dealt with in a future publication.

In the right panels of Fig. 6 we show the particle velocities after 10 Gyr of simulations. While we clearly see that the quantized nature in the W-component has washed out (see above) a new feature has appeared. In all our simulations we see over- and under-densities in the azimuthal V-velocities. This quantization is not as sharp as formerly seen in W but still clearly visible. We call this feature azimuthal fish, because of its form. We believe that this quantization is the direct counterpart of the density enhancements in tidal tails which are reported by Küpper et al. (2010). The only difference between their and our models is that they investigate slowly evolving globular clusters (GCs), which loose their mass slowly over long time-intervals, while our models have dissolved rapidly and the stars spread out much faster and wider than seen in Küpper et al. (2010). We will investigate this problem further and report about it in a follow up paper.

4 CONCLUSIONS

We compute models of dissolving embedded star clusters on circular orbits around the MW. The aim of our study is to investigate if SCs of different mass, SFE and gas-expulsion time can support not only the distribution of stars and their velocities in the thin disc of the MW but also in the thick disc.

We also co-added the results of our simulations to show the effect of a whole population of SCs, following a standard ICMF, to the distribution of stars in the discs of the MW.

We can summarize the results of our models in the following points:

- The stars of dissolved SCs form density distributions in the z-direction which can be best fitted by exponential profiles.
- While low-mass SCs (masses of the order of 10^4 and 10^5 $M_\odot$) contribute only to a component similar to the thin disc of the MW, high mass clusters(masses $> 10^5$ $M_\odot$) show distributions which can be described best by two exponential profiles and therefore their stars contribute into two components similar to the thin and thick disc of the MW.
- The velocity dispersion of the stars distributed into the thin component show a much lower velocity dispersion than the actual dispersion of the thin disc of the MW. This may be due to the fact that we do not take any other mechanisms to enhance the velocity dispersion into account (e.g. spiral arms, giant molecular clouds, other SCs, ...)
- The thick component of our model shows a velocity dispersion which is higher than observed in the MW thick disc. We therefore conclude that inside the MW disc SCs with masses comparable to 10^7 $M_\odot$ might never have formed. The thick component of our 10^6 $M_\odot$ model has enough velocity dispersion to explain the thick disc. This is in nice agreement with the analytical results of Kroupa (2002).

We need to discuss these findings a bit further. On the first glance it seems to be rather odd that stars of one dissolved star cluster should spread into two distinct distributions with two distinct velocity dispersions. The density distribution of all our dissolved clusters exhibits a very distinct profile showing a 'peak' around small z-distances and a kind of 'envelope' of large z-distances. The transition between these two parts is rather continuous and not sharp. We see that for low-mass clusters the 'peak' is more pronounced than the 'envelope' and therefore they can be fitted best by a single exponential profile. Also the stars in the 'envelope' do not extend to z-heights comparable to the thick disc. For high-mass clusters we see a very substantial 'envelope', reaching out to high z-distances, and therefore are better described by two exponentials. The same is true for the distribution of W-velocities. The distribution is similar in shape to the distribution of velocities found in stars in the solar neighbourhood. It is neither a single nor a double Gaussian but rather a continuous overlay of many Gaussians. Nevertheless, the usual observational procedure to analyse these distributions is to fit two Gaussians to the probability plot and assigning two velocity dispersions to it - one for the thin disc component and one for the thick disc component. So we followed the same method. Again for low-mass clusters there are no stars with high velocities and therefore we only assign one velocity dispersions to their distributions.

Another issue, which needs to be discussed, is the constant analytical potential used in this study. It is clear that in the distant past the disc(s) of the MW were much smaller in mass and maybe in size. A 'popping' star cluster would spread its stars to much larger

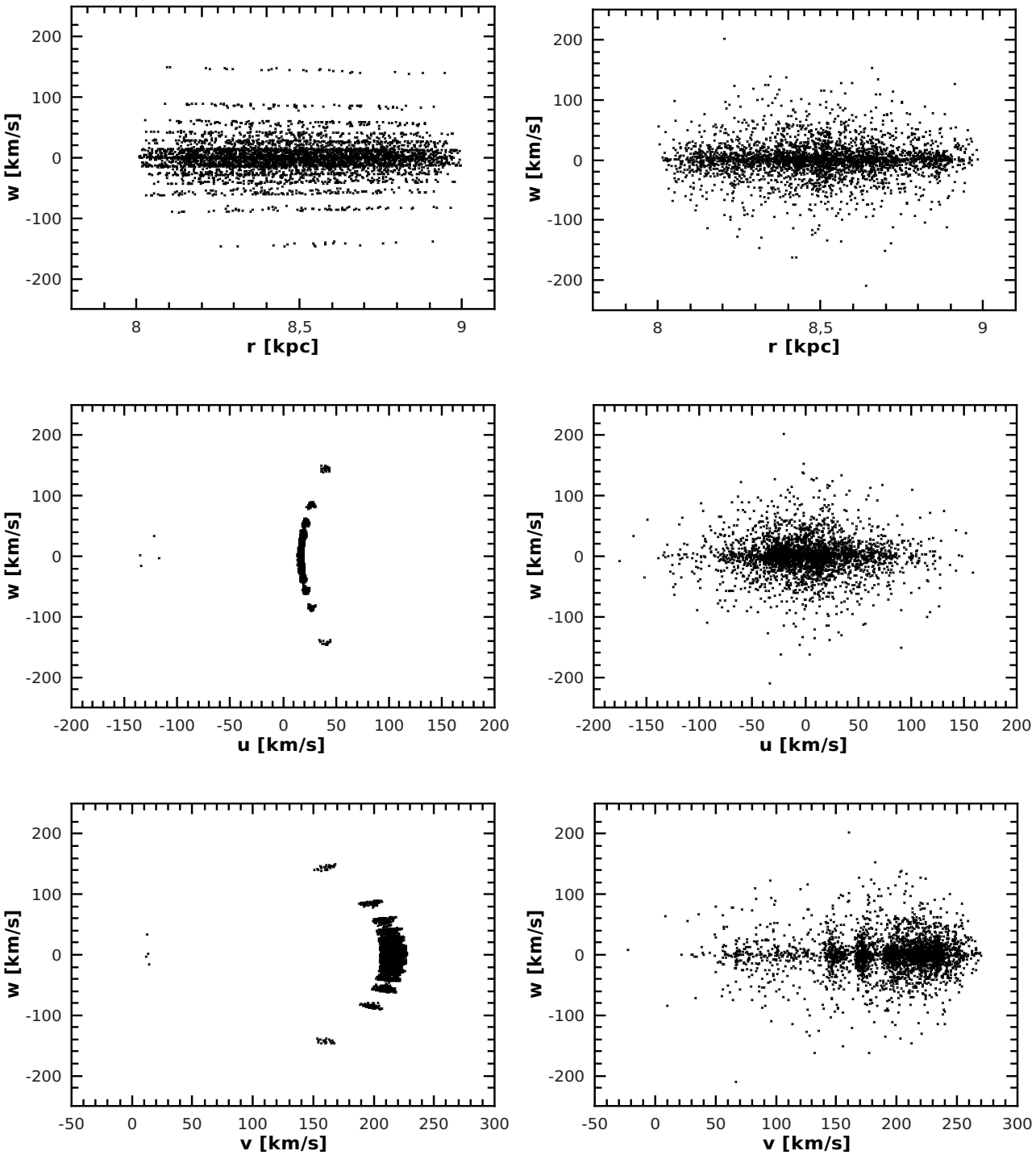

Figure 6. Evolution of a model SC in velocity space. Left panels show the velocity distributions after 270 Myr (≈ one revolution round the Galaxy). Right panels show the distributions at the end of the simulation (10 Gyr). From top to bottom we show W against R, W against U and finally W against V. Top left panel shows clearly the quantized nature of the W-velocities which lead to the so-called Christmas-tree effect. At the lower right panel we see the 'azimuthal fish'.

z-heights much more easily. So it would rather help our scenario to explain the thick disc. Furthermore the adiabatic heating of stars due to the growth in mass of the MW will enhance the velocity dispersion of the stars and bring them onto orbits with higher z-distances.

Besides, it is well known that the thick disc and thin disc components have a different chemical history. The ratios of α-(O,Mg,Si,Ca, and Ti) elements, for example, are higher for stars in the thick disc than for stars of the thin disc at given metallicity (Bensby et al. 2007; Kobayashi et al. 2011). This indicates a

short star formation time-scale in which enrichment is dominated by Type II supernovae (SNe II) (Alves-Brito et al. 2010). Supernovae events guide the gas expulsion process, that together with all the other scattering mechanisms, might also help to move stars from the 'peak' structure into the 'envelope' structure. This would explain the problem that we do not see stars with thick disc chemical properties amongst thin disc stars and, therefore, why we see different populations of stars with different chemical properties in the thin and thick disc of our MW now. Another possibility would be if the MW saw an early epoch of star formation, where the formation of low-mass clusters was suppressed (in comparison with the evidence for this from top-heavy galaxy-wide initial mass functions of stars in young galaxies Weidner et al. 2010).

We therefore are able to show that one does not need any merger scenarios to explain the structure of the MW disc. The simple assumption that all stars form in SCs is enough to explain the thin as well as the thick disc of our MW, thus confirming the analytical calculations by Kroupa (2002) rather nicely. These models are applied by Kroupa (2002) as a possible explanation not only of the thick disk, but also of the observed but hitherto not understood secular heating of the thin disk. Here the notion raised is that the observed thickening of the MW thin disk with age may be due to a falling star-formation rate (SFR) since the past 10 Gyr, whereby a small SFR implies the formation of SCs with small masses (Weidner & Kroupa 2004).

While conducting our experiments we detected two new effects within the distributions of the stars. After about one revolution around the Galaxy the stars have spread in the z-direction in to a form that has striking similarities to a Christmas-tree. As the discovery was made shortly before Christmas we called the effect officially Christmas-tree distribution. At the same time the distribution of W-velocities seems to have only certain discrete values. This feature is transient and disappears after several revolutions about the MW. We suspect that this is the case when the leading and trailing arms wrap completely around the Galaxy and overlap at the former SC position. Then the velocities of the leading arm fall into the gaps of the velocity distribution of the trailing stars. The reason to see a peculiar distribution like the Christmas-tree in the first place is still not fully investigated and will be dealt with in a follow-up paper. We suspect that we see a similar behaviour in z as is reported by Küpper et al. (2010) along the tidal tails.

The second effect showed up towards the end of our simulations. This effect consists of peculiar over- and under-densities in the V velocities which show a pattern that reminded us of a fish. We therefore called this effect the azimuthal fish. Even though the 'tidal tails' of the dissolved star clusters are well mixed towards the end of the simulations so that we can not see any density variations in the positions, we believe that our fish pattern is directly related to the slowly evolving tidal tails of GCs and their density variations. As the quantized velocities associated with the Christmas-tree we see now the left-over velocity signatures of a similar effect in azimuthal direction., while the positional counterpart is not visible due to the fast evolution of our models. Also this effect will be investigated further and reported about in a following publication.

As a final comment we state again that our models are able to reproduce the structural features of the MW. Our models add therefore another possible explanation of how the discs of the MW and similar galaxies may have acquired their properties. Which theory will be right - future observation might tell or even show that we might deal with a superposition of all theories at the same time.

Acknowledgments: PA is supported through a Chilean CONICYT grant and a Deutscher Akademischer Austauschdienst (DAAD) grant. MF acknowledges support through FONDECYT project no. 1095092.

REFERENCES

Abadi M. G., Navarro J. F., Steinmetz M., Eke V. R., 2003, ApJ, 597, 21
Alves-Brito A., Meléndez J., Asplund M., Ramirez I., Yong D., 2010, A&A, 513, A35
Bell E.F., et al. 2008, ApJ, 680, 295
Bensby T., Feltzing S., Lundström I., 2003, A&A, 410, 527
Bensby T., Zenn A. R., Oey M. S., Feltzing S., 2007, ApJ, 663, L13
Bochanski J., Munn J., Hawley S., West A., Covey K., Schneider D., 2007, AJ, 134, 2418
Bournaud F., Elmegreen B. G., Elmegreen D. M., 2007, ApJ, 670, 237
Brook C. B., Gibson B. K., Martel H., Kawata D., 2005, ApJ, 630, 298
Fellhauer M., Kroupa P., Baumgardt H., Bien R., Boily C.M., Spurzem R., Wassmer N., 2000, New Ast., 5, 305
Fuchs B., Dettbarn C., Jahreiss H., Wielen R. 2001, in Deiters S. et al., eds, ASP Conf. Ser. Vol. 228, STAR2000: Dynamics of Star Clusters and the Milky Way. Astron. Soc. Pac,. San Francisco, p.235
Hammer F., Puech M., Chemin L., Flores H., Lehnert M.D. 2007, ApJ, 662, 322
de Jong J.T.A., Yanny B., Rix H.-W., Dolphin A.E., Martin N.F., Beers T.C. 2010, ApJ, 714, 663
Juric M., et al. 2008, ApJ,673, 864
Kazantzidis S. et al., 2008, ApJ, 688, 254
Kobayashi C., Karakas A.I., Umeda H. 2011, MNRAS, in press, arXiv:1102.5312v1
Kroupa P. 2002, MNRAS, 330, 707
Kroupa, P. 2008, The Cambridge N-Body Lectures, LNP, 760, 181
Kroupa, P., Aarseth, S., Hurley, J. 2001, MNRAS, 321, 699
Kroupa P., Boily C.M., 2002, MNRAS, 336, 1188
Küpper A.H.W., Kroupa P., Baumgardt H., Heggie D.C. 2010, MNRAS, 401, 105
Lada C. J., Lada E. A., 2003, ARA&A, 41, 57
Melèndez J., et al. 2008, A&A, 484, L21
Plummer, H. C., 1911, MNRAS, 71, 460
Quinn P. J., Hernquist L., Fullagar D. P., 1993, ApJ, 403, 74
Roŝkar R., Debattista V. P., Stinson G. S., Quinn T. R., Kaufmann T., Wadsley J., 2008, ApJ, 675, L65
Schönrich R., Binney J., 2009, MNRAS, 399, 1145
Soubiran C., Bienaymé, O., Siebert, A. 2003, A&A, 398, 141
Vallenari A., Pasetto S., Bertelli G., Chiosi C., Spagna A., Lattanzi M., 2006, A&A, 451, 125
Veltz L., Bienaymé O., Freeman K. C. et al., 2008, A&A, 480, 753
Villalobos A., Helmi A., 2008, MNRAS, 391, 1806
Weidner C., Kroupa P., 2004, MNRAS, 348, 187
Weidner, C., Kroupa, P. and Pflamm-Altenburg, J. 2011, MNRAS, in press, arXiv:1011.3814
Whitmore B.C., Zhang Q., Leitherer C., Fall S.M., Schweizer F., Miller B.W., 1999, AJ, 118, 1551